Acta Otolaryngol (Stockh) 1989; Suppl. 467: 249–256

CHAPTER 30

# Models of Nonlinear Vibration. II. Oscillator with Bilinear Stiffness

MALVIN C. TEICH,[1] SUZANNE E. KEILSON[1] and SHYAM M. KHANNA[2]

*Columbia University, Departments of [1]Applied Physics and [2]Otolaryngology, New York, USA*

## INTRODUCTION

In the previous paper we introduced the bilinear resistance oscillator (Keilson, Teich and Khanna, 1989a). In this paper we continue our investigation into the behavior of simple bilinear oscillators with a study of the bilinear stiffness oscillator. The general approach and numerical methods used to study such dynamical systems were described in the previous paper, and have been considered in other references in the field of nonlinear dynamics (Thompson and Stewart, 1986; Berge, Pomeau and Christian, 1986). The bilinear stiffness oscillator exhibits a stiffness with value $k_1$ when the displacement is positive with respect to an arbitrary origin, and $k_2$ when it is negative with respect to that origin. Such simple deterministic systems have enough degrees of freedom to exhibit complex behavior, such as subharmonic resonances and chaotic motion. The bilinear mass model is treated in a companion paper (Keilson, Teich and Khanna, 1989b).

The bilinear stiffness oscillator has been considered previously in the context of marine engineering. The dynamic motions of a mooring buoy and line attached to a massive supertanker, and driven by steady ocean waves, were modeled by a one-dimensional oscillator with a stiffness discontinuity (Thompson and Stewart, 1986; Thompson and Ghaffari, 1983; Thompson, Bokaian and Ghaffari, 1984). These studies have shown that true chaotic motion can occur only in the case when one of the stiffness values becomes infinite, in which case it is refered to as an impact oscillator (Thompson and Ghaffari, 1983; Thompson, Bokaian and Ghaffari, 1984).

One-dimensional, forced (non-autonomous) oscillators of this kind may serve as useful models for elements of the cochlear transduction process. One example is a simplified model for the asymmetrical motion of the stereocilia bundle atop the hair cell, which is known to exhibit a displacement-dependent stiffness (Flock and Strelioff, 1984; Hudspeth and Howard, 1988).

## THEORY

The equation of motion of a bilinear stiffness oscillator is

$$mx''(t)+rx'(t)+k(x)\,x(t) = A_o \cos(2\pi f_s t), \tag{1}$$

where x, x′, and x″ represent the displacement, velocity, and acceleration, respectively, and the coefficients m, r, and k represent the mass, resistance, and stiffness, respectively. This is an ordinary, nonlinear, nonautonomous differential equation since the stiffness coefficient k(x) is a function of the displacement x and the time t appears as an explicit variable in the forcing function. The forcing function has an amplitude $A_o$ and a frequency $f_s$. For the bilinear stiffness oscillator,

$$\begin{aligned} k(x) &= k_1 \quad \text{for } x \geq 0 \\ k(x) &= k_2 \quad \text{for } x < 0. \end{aligned} \tag{2}$$

One can define a bilinear period of the motion T, that is an average of the two periods associated with each domain of motion. There is a corresponding bilinear frequency $f_c$. Because of the relationship between the natural frequency of a system and its stiffness, one can also define an equivalent stiffness K that is a combination of the two k's. These parameters turn out to be (Thompson and Stewart, 1986)

$$T = (T_1+T_2)/2, \tag{3}$$

$$f_c = 1/T = (1/2\pi)\,(K/m)^{1/2}, \tag{4}$$

and

$$K = 4k_1 k_2/(k_1^{1/2}+k_2^{1/2})^2. \tag{5}$$

As a result of the form of Eq. (2), the solution scales linearly with the amplitude of the forcing function $A_o$ so that the normalized displacement and velocity, and their spectra, do not change with the applied signal level. For the case of arbitrary k(x) the solution does not in general scale linearly with $A_o$ so that the results will depend on the amplitude of the forcing function.

Results are shown in the form of displacement waveforms and their Fourier spectra, velocity waveforms and their spectra, phase-space projections, and plots of the velocity harmonics as a function of signal frequency. The integration was always started with the initial conditions $x(0)=x'(0)=0$. Startup transients were removed by first integrating for 10,000 steps before storing the solutions. The time course of the stored solution was sufficiently long so that convergence to a limiting motion could usually be observed empirically. The spectra were obtained by a fast-Fourier transform (FFT) operation on the discrete array containing the sampled time waveform.

## RESULTS

Solutions for the sinusoidally forced bilinear stiffness oscillator were obtained by using the values $A_o=100$ dynes, $m=1\times10^{-6}$ g, $k_1=10$ dyne/cm, $k_2=2$ dyne/cm, and $r=0.001$ dyne-sec/cm in Eqs. (1) and (2). The solutions presented are representative and not peculiar to this choice of parameters. The best frequency of this oscillator is given by $f_c=317$ Hz [see Eq. (5)]. This was chosen to be the same as the best frequency of the bilinear resistance oscillator (Keilson, Teich and Khanna, 1989a) and the bilinear mass oscillator (Keilson, Teich and Khanna, 1989b).

In Figures 1–4, results are shown in the form of (a) displacement waveforms, (b) displacement waveform spectra, (c) velocity waveforms, (d) velocity waveform spectra, and (e) phase-space projections. Figure 1 shows data at $f_s=73$ Hz, below the CF; Figure 2 shows data at $f_s=317$ Hz (at CF); Figures 3 and 4 show data at $f_s=610$ and 806 Hz, respectively, above CF.

Examining the displacement waveform at the four frequencies indicates that the deviation of the waveshape from sinusoidal is substantial well below CF and generally decreases as the signal frequency increases. However, a strong subharmonic resonance emerges above CF, as is evident in Figure 3. For the initial conditions chosen, all of the displacement waveforms are more-or-less restricted to the domain of negative displacement, thereby exhibiting strong rectification (negative dc offset). Consistent with the general trend of the behavior of the displacement waveforms, the number of harmonic components present in the displacement spectra decreases with increasing signal frequency.

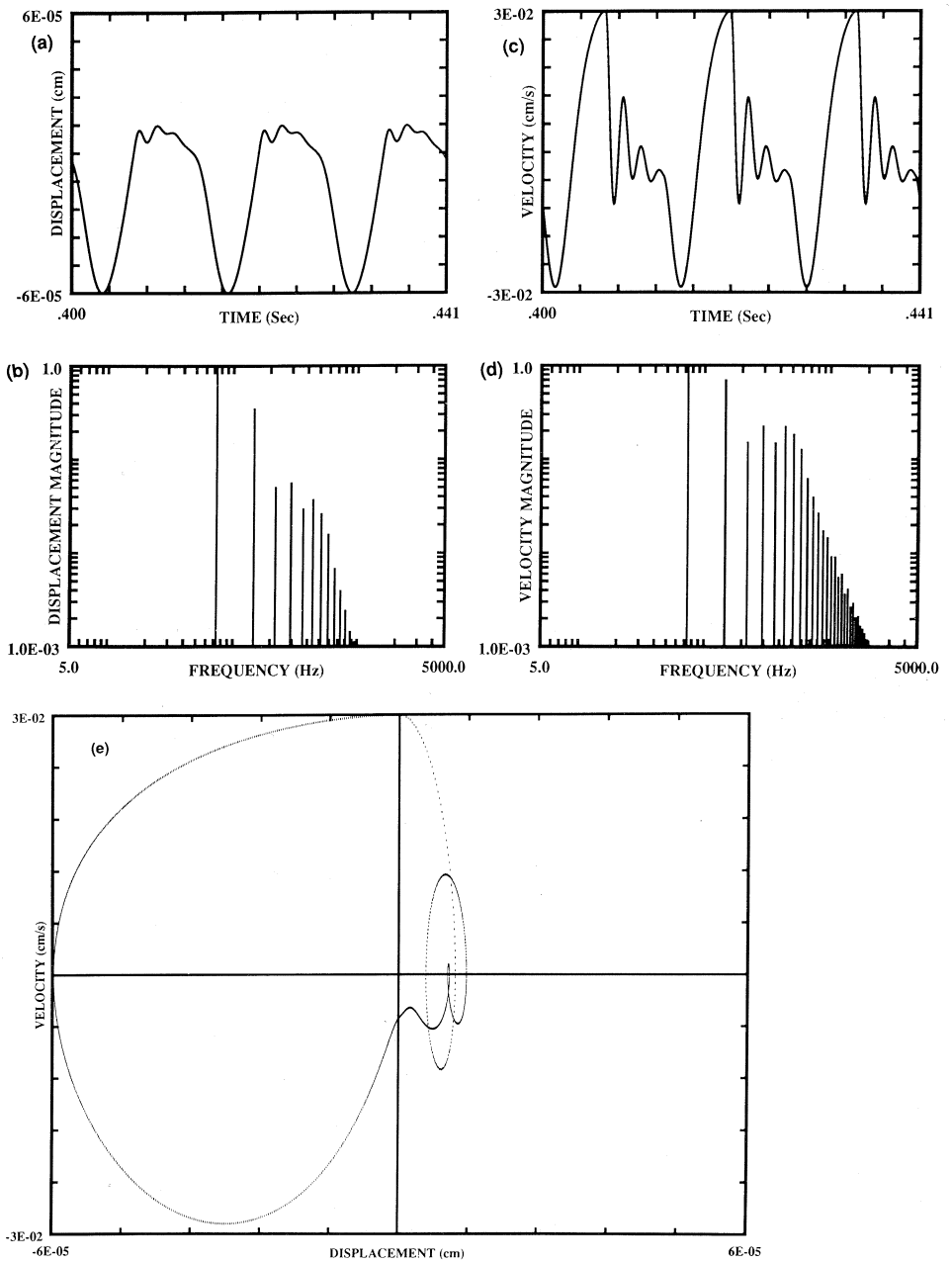


*Fig. 1.* Response of the bilinear stiffness oscillator to a signal frequency $f_s$=73 Hz (below CF). (a) Time waveform of the displacement. The response is distinctly nonsinusoidal, exhibiting a high frequency oscillation at its positive peaks. The response favors negative displacements so that there is a negative dc offset. (b) Fourier spectrum of the displacement waveform. The large number of harmonics (12 are visible) confirms the nonsinusoidal nature of the waveform. The ratio of the displacement magnitude at dc (not shown) to the magnitude at the signal frequency is 0.87. (c) Time waveform of the velocity. The waveform deviates most from sinusoidal behavior as it oscillates about the zero crossing. (d) Fourier spectrum of the velocity waveform. The velocity, being the derivative of the displacement, exhibits a greater number of high-frequency harmonics. (e) Phase-space projection. The trace is distinctly non-elliptical and asymmetric for both positive and negative displacements and velocities. The small loops in the positive displacement represent the "ringing" of the waveform with high frequency harmonics.

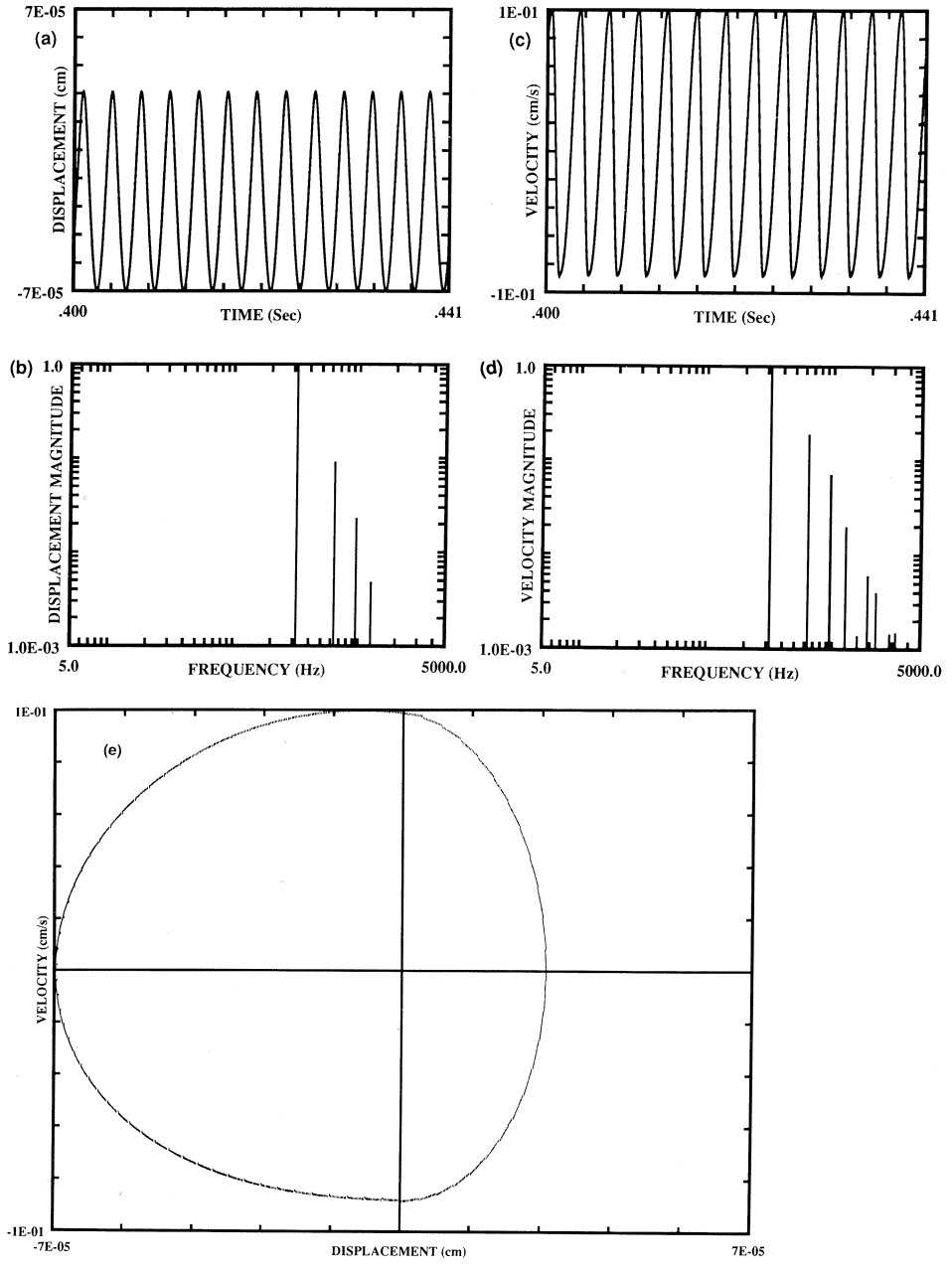


*Fig. 2.* Response of the bilinear stiffness oscillator to a signal frequency $f_s$=317 Hz (at CF). (a) Time waveform of the displacement. The response appears to be quite sinusoidal, but with a large negative dc offset. (b) Fourier spectrum of the displacement waveform; four harmonics are readily seen. The ratio of the displacement magnitude at dc to the magnitude at the signal frequency is 1.03. (c) Time waveform of the velocity. Here the response appears with unequal excursions into the positive and negative domains. (d) Fourier spectrum of the velocity waveform. Again, a greater number of high-frequency harmonics are seen than in the displacement spectrum. (e) Phase-space projection. The trace, which is non-elliptical, shows more symmetry for positive and negative velocities than for positive and negative displacements.

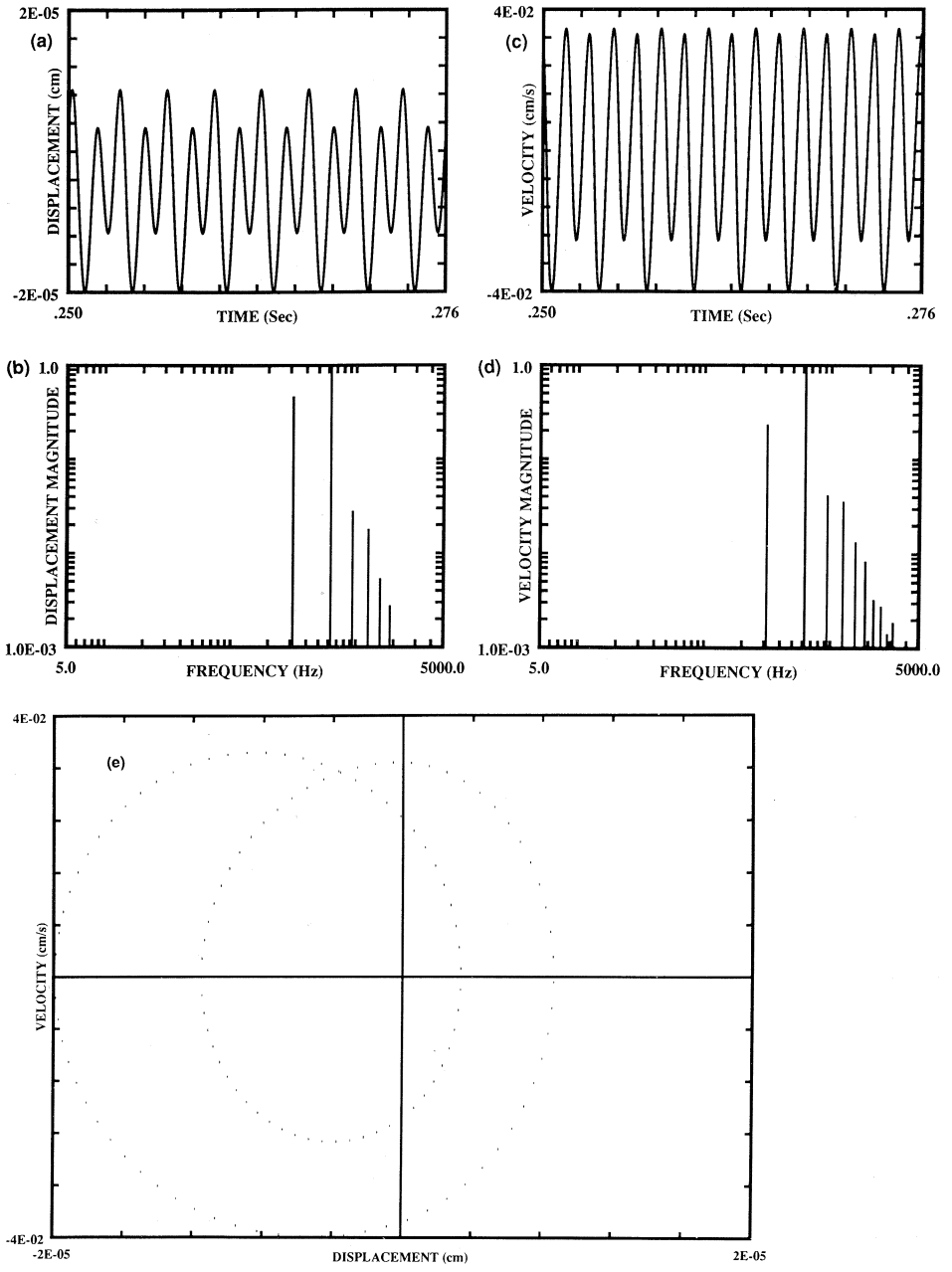


*Fig. 3.* Response of the bilinear stiffness oscillator to a signal frequency $f_s$=610 Hz (above CF). (a) Time waveform of the displacement. The response appears periodic but with a strong component at ~$f_s/2$ and a negative dc offset. (b) Fourier spectrum of the displacement waveform. Four harmonics of $f_s$ are readily seen, and a strong spectral component below the signal frequency appears at about 300 Hz, which is also near the CF of the oscillator. This is the subharmonic response. The ratio of the displacement magnitude at dc to the magnitude at the signal frequency is 0.97. (c) Time waveform of the velocity. Again, the period of the sinusoidal behavior is doubled because there is a large response at the CF ~$f_s/2$. (d) Fourier spectrum of the velocity waveform. Seven harmonics are visible. (e) Phase-space projection. The trace shows a loop that represents the strong subharmonic resonance. The response is still largely restricted to negative values of the displacement.

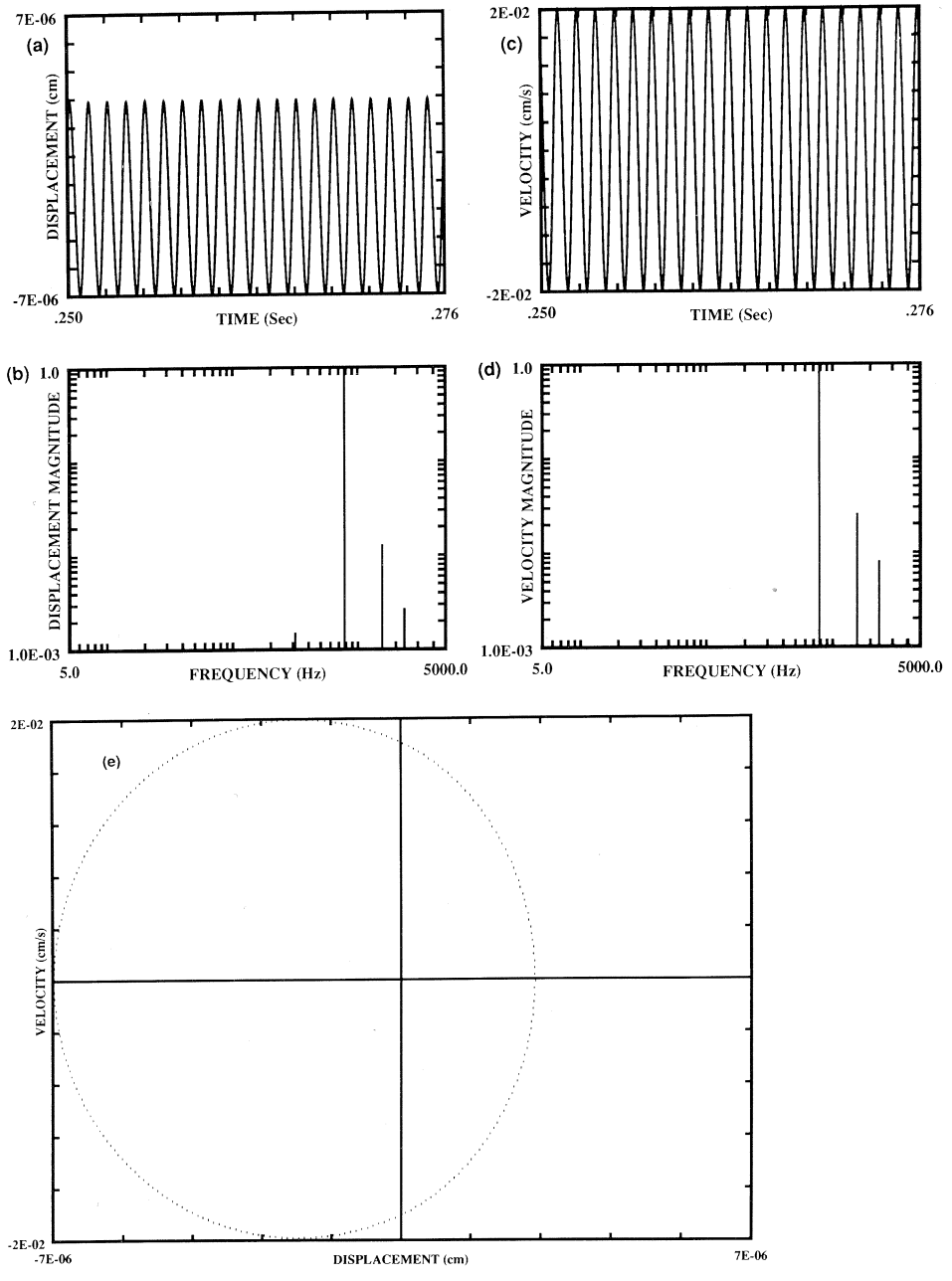


*Fig. 4.* Response of the bilinear stiffness oscillator to a signal frequency $f_s$=806 Hz (well above CF). (a) Time waveform of the displacement. The response appears to be quite sinusoidal but with a large negative dc offset. This is another example of the rectification of displacement waveforms that occurs at all signal frequencies. (b) Fourier spectrum of the displacement waveform. Two harmonics are clearly visible. The ratio of the displacement magnitude at dc to the magnitude at the signal frequency is 0.92. (c) Time waveform of the velocity. It appears quite sinusoidal and with equal excursions in the positive and negative domains.(d) Fourier spectrum of the velocity waveform. Two harmonics can be seen. (e) Phase-space projection. The trace appears circular but is also asymmetric in its positive and negative displacements.

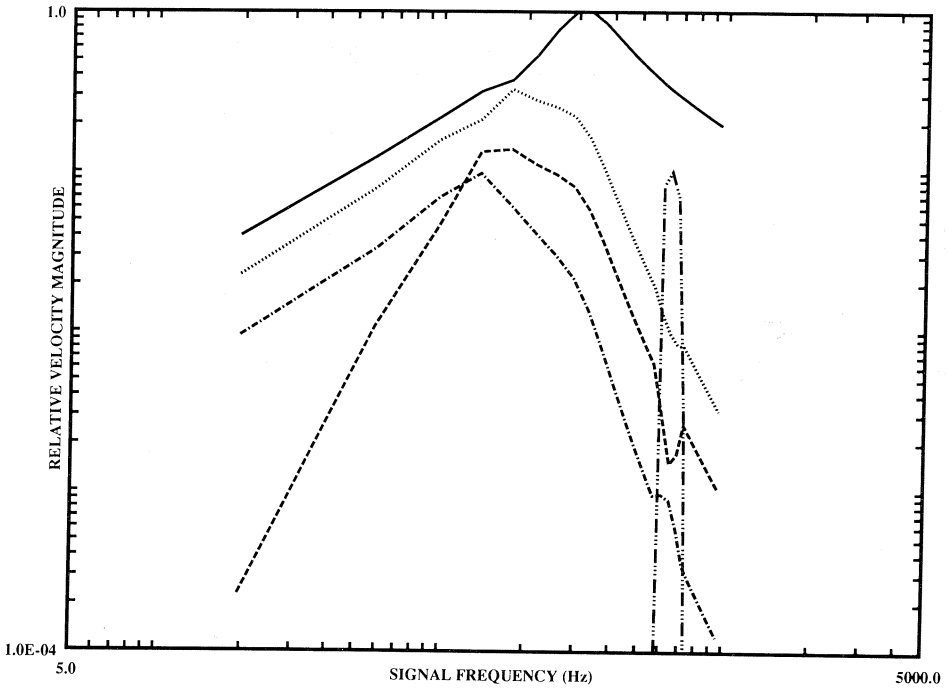


*Fig. 5.* Relative velocity-magnitude frequency-response curves for the bilinear stiffness oscillator. The curves represent the magnitude of the first four velocity harmonics, and a sharply tuned subharmonic resonance, plotted as a function of the applied signal frequency. The curves are coded as follows: fundamental (solid curve), 2nd harmonic (dotted curve), 3rd harmonic (dashed curve), 4th harmonic (dash-dot curve), and subharmonic (dash-three-dots curve).

This is not the case for the velocity waveforms which have a more symmetrical excursion. Since the velocity is the derivative of the displacement, however, the rapid but small displacement oscillations in the domain of positive displacement are greatly enhanced. These oscillations appear near the zeroes of velocity. This is in contrast to the bilinear resistance oscillator where velocity oscillations appear near the peaks in the velocity waveform (Keilson, Teich and Khanna, 1989a). The velocity spectra follow the same trend as the displacement spectra with increasing signal frequency, but they always show more harmonic components.

The phase-space projections evidence nonelliptical and asymmetric behavior at all signal frequencies. When the two stiffness values differ only slightly, the distortions from ellipticity are relatively small. As the stiffness ratio increases, the oscillator behaves as an unusual type of rectifier. In the domain of the larger stiffness, the positive displacement excursion is severely limited; the motion is largely confined to the domain of the lower stiffness. The oscillator then spends a greater proportion of its time in this domain. As a natural consequence of its dynamics, the bilinear stiffness oscillator therefore rectifies displacement waveforms at a constant fraction of their range. This kind of behavior had to be artificially introduced in the linear-filter/static-rectifier model considered earlier (Teich, Keilson and Khanna, 1989). The subharmonic resonance is manifested as a large loop in the phase-space projection of Figure 3(e).

The relative magnitudes of the first four velocity harmonics are shown as a function of signal frequency in Figure 5. These illustrate that the velocity tuning observed at the fundamental frequency is quite different from that observed at the second, third, and

fourth harmonics. The frequencies of maximal response (best frequencies) of the second and third harmonics lie below that of the fundamental. All of the harmonic tuning curves exhibit rather subtle multiple sub-peaks. For this set of parameters, the low-frequency slopes of the second and fourth harmonic follow that of the fundamental, whereas the high-frequency slopes are steeper than that of the fundamental. The third harmonic curve rises much more steeply and crosses the fourth-harmonic curve.

## CONCLUSION

For the bilinear stiffness oscillator model, the number and magnitude of the harmonic components in the displacement and velocity spectra are maximal at a signal frequency below CF and decrease with increasing signal frequency. A sharply tuned subharmonic resonance appears when the signal frequency is near, but not necessarily precisely at, a multiple of the CF. The displacement waveforms exhibit substantial rectification at all signal frequencies.

## ACKNOWLEDGEMENTS

This work was supported by the National Institutes of Health and the National Science Foundation.

## REFERENCES

Berge P, Pomeau Y, Christian V (1986). Order within chaos. New York: Wiley & Sons.

Flock Å, Strelioff D (1984). Stiffness of sensory-cell hair bundles in the isolated guinea pig cochlea. Hearing Research 15: 19–28.

Hudspeth AJ, Howard J (1988). Compliance of the hair bundles associated with gating of mechano-electrical transduction channels in the bullfrog's saccular hair cell. Neuron 1: 189–199.

Keilson SE, Teich MC, Khanna SM (1989a). Models of nonlinear vibration. I. Oscillator with bilinear resistance. Acta Otolaryngol (Stockh) Suppl 467: 241–248.

Keilson SE, Teich MC, Khanna SM (1989b). Models of nonlinear vibration. III. Oscillator with bilinear mass. Acta Otolaryngol (Stockh) Suppl 467: 257–264.

Teich MC, Keilson SE, Khanna SM (1989). Rectification models in cochlear transduction. Acta Otolaryngol (Stockh) Suppl 467: 235–240.

Thompson JMT, Bokaian AR, Ghaffari R (1984). Subharmonic and chaotic motions of compliant offshore structures and articulated mooring towers. ASME J Energy Resources Technology 106: 191–198.

Thompson JMT, Ghaffari R (1983). Chaotic dynamics of an impact oscillator. Phys Rev A 27: 1741–1743.

Thompson JMT, Stewart HB (1986). Nonlinear dynamics and chaos. New York: Wiley & Sons.